COBEM 2021 26th International Congress of Mechanical Engineering
November 22-26, 2021, Virtual Congress, Brazil
ABCM Associação Brasileira de Engenharia e Ciências Mecânicas

COB-2021-XXXX
ANALYSIS OF WAVE PROPAGATION IN ORIGAMI-LIKE STRUCTURES

Edilson Dantas Nóbrega
Vilson Souza Pereira
Dalmo Inácio Galdez Costa
Federal University of Maranhão, UFMA-CCET-CCEM, Cidade Universitária Dom Delgado, São Luís - MA, Brazil.
edilson.dantas@ufma.br, vilson.sp@ufma.br, dalmo.costa@ufma.br

José Maria Campos dos Santos
University of Campinas, UNICAMP-FEM-DMC, Rua Mendeleyev 200, Cidade Universitária Zeferino Vaz, Campinas - SP, Brazil.
zema@fem.unicamp.br

Abstract. *Periodic structures made of identical patterns (phononic crystals - PCs), with the purpose of obtaining certain desired phenomena known as band gaps, have gained great interest in modern engineering. Although the efficiency of PC structures has been analyzed in several experimental ways, an explanation of the influence of pattern topology on wave propagation properties is still lacking. This work focuses on analyzing the propagation of waves along a periodic structure of the origami type. In this model, longitudinal and flexural movements are incorporated. The elements are connected at a certain angle to form two sides of a triangular geometry. A parametric analysis is proposed to analyze the influence of the coupling angle, as well as the length of the frame elements. The dispersion curves of the wave propagation modes of the structure were also investigated.*

Keywords: *wave propagation, band gaps, phononic crystals, dispersion diagram, periodic structures.*

1. INTRODUCTION

Study of wave propagation on periodic structures started in mid-70 with the researches of Mead (1970, 1973) and have gained much attention ever since. This area of research has several applications such as vibration and noise control, health monitoring and so on. Phononic Crystals (PC) are structural systems that exhibits a degree of spatial periodicity, in this type of material a cell is defined and then repeated periodically, in order to display some specific desired behavior (Hussein *et al.*, 2014). This type can also be defined as artificially periodic composite materials that are based on a difference between the receptance of their constituent materials in order to generate bandgaps Nanda and Karami (2018). This phenomenon is observed in some frequency ranges where no sounds or vibrations are allowed to propagate. In order to achieve this, one needs to model a cell as an elastic structure that changes material or cross-section area along its length, then apply periodicity condition.

In terms of analysis, the Floquet-Bloch's theorem can be used to obtain a transfer matrix eigenproblem, which the solution provides attenuation and wave-modes. This method has been applied in various types of spectral elements (SE) models, simple ones such as rods and beams ((Nobrega *et al.*, 2016; Goto *et al.*, 2020)), and more complex ones such as plates and shells (Miranda *et al.*, 2019, 2020; Pereira and Santos, 2021), including different material properties or even shunt piezoelectric structures, couplings, and mediums (Silva *et al.*, 2013; Chen *et al.*, 2020). In P B Silva *et al.* (2011) analytical spectral element for periodic rods is applied to observe the effect of wave propagation in the audio frequency range. The existence of band gaps in the dynamic responses is demonstrated and an experimental test is performed to validate the numerical results. In Xiao *et al.* (2012), metamaterial based elastic rods containing periodically attached multi-degree-of-freedom spring-mass resonators are investigated. A methodology based on a combination of the spectral element method and the Bloch theorem is developed, yielding an explicit formulation for the complex band structure calculation which is called Wave Spectral Element (WSE) method. Investigation on band gaps grew up in recent years, and researchers started to apply this methods for various configurations. In Xiao *et al.* (2013), vibration band gaps in a phononic crystal (PC) Euler-Bernoulli beam on a foundation model is investigated theoretically using the combination of transfer matrix (TM) method and Bloch theorem .

Due to its building characteristics, deployable (Nanda and Karami, 2018) and origami like structures provides an interesting field for designing configurations that meets particular needs (Lv *et al.*, 2014), among them tuning specific frequency ranges for band gaps by controlling certain geometric parameters.

In this paper we proposed to analyze wave propagation in a structure generated by coupling waveguides which alternate spacial orientation to form a PC frame. Figure 1 shows a PC frame scheme with n cells.

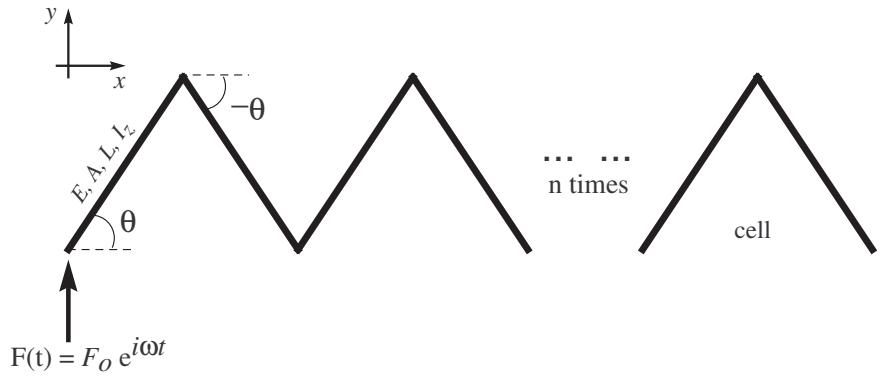

Figure 1. Schematic representation of a origami-like structure. This frame is built through the combination of "n" triangular cells.

2. ORIGAMI-LIKE STRUCTURE

2.1 Dynamic stiffness matrix

Figure 2 shows a representative origami cell (ROC) isolated from the complete periodic plane structure of the example in Figure 1. The ROC consists of two connected members of length L and rotation angle θ.

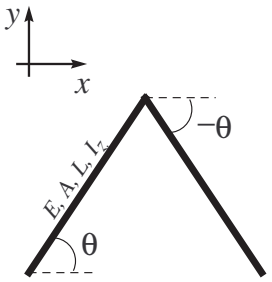

Figure 2. Cell with only one material type organized in a triangular shape.

The structure members in ROC were represented by the rod and beam models. Assuming that the structural members in the ROC shown in Figure 2 are all clamped at the joints, we will represent them using frame models, which take the longitudinal and flexural vibrations simultaneously. The spectral element model for the axial-bending beam model can be obtained by combining the rod and beam spectral element, given by the following equations.

Dynamic equilibrium equation for a ROC can be written as

$$\mathbf{S_f u} = \mathbf{F}, \tag{1}$$

where $\mathbf{S_f}$ is the spectral dynamic stiffness matrix of a frame that is composed by a junction of the rod (S_r) and beam (S_b) matrices. Dynamic stiffness matrix for a rod is given by (Lee, 2009):

$$\mathbf{S_r}(\omega) = \frac{A\,E\,\mathbf{k_r}}{\sin(L\,\mathbf{k_r})} \begin{bmatrix} cos(L\,\mathbf{k_r}) & -1 \\ -1 & cos(L\,\mathbf{k_r}) \end{bmatrix}, \tag{2}$$

and

$$\mathbf{k_r}(\omega) = \sqrt{\frac{\omega^2 \rho}{E}} \tag{3}$$

where $\mathbf{k_r}$ is the wave number of a rod, A, E and L are the cross-section area, Young's modulus and length of a structural member, respectively. The matrix for a beam is given by (Lee, 2009):

$$\mathbf{S_b}(\omega) = \frac{E\,I}{L^3} \begin{bmatrix} S_{b11} & S_{b12} & S_{b13} & S_{b14} \\ S_{b12} & S_{b22} & S_{b23} & S_{b24} \\ S_{b13} & S_{b23} & S_{b33} & S_{b34} \\ S_{b14} & S_{b24} & S_{b34} & S_{b44} \end{bmatrix}, \tag{4}$$

with

$$\begin{array}{lcl} S_{b11} & = & S_{b33} = \Delta_b\, \bar{\mathbf{L}}^3(\cos(\bar{\mathbf{L}})\sinh(\bar{\mathbf{L}}) + \sin(\bar{\mathbf{L}})\cosh(\bar{\mathbf{L}})) \\ S_{b22} & = & S_{b44} = \Delta_b\, \bar{\mathbf{L}}^3\, \mathbf{k}_b^{-2}(-\cos(\bar{\mathbf{L}})\sinh(\bar{\mathbf{L}}) + \sin(\bar{\mathbf{L}})\cosh(\bar{\mathbf{L}})) \\ S_{b12} & = & -S_{b34} = \Delta_b\, \bar{\mathbf{L}}^3\, \mathbf{k}_b^{-1}(\sin(\bar{\mathbf{L}})\sinh(\bar{\mathbf{L}})) \\ S_{b13} & = & -\Delta_b\, \bar{\mathbf{L}}^3(\sin(\bar{\mathbf{L}}) + \sinh(\bar{\mathbf{L}})) \\ S_{b14} & = & -S_{b23} = \Delta_b\, \bar{\mathbf{L}}^3\, \mathbf{k}_b^{-1}(-\cos(\bar{\mathbf{L}}) + \cosh(\bar{\mathbf{L}})) \\ S_{b24} & = & \Delta_b\, \bar{\mathbf{L}}^3\, \mathbf{k}_b^{-2}(-\sin(\bar{\mathbf{L}}) + \sinh(\bar{\mathbf{L}})) \\ \Delta & = & \frac{1}{1-\cos\bar{\mathbf{L}}\cosh\bar{\mathbf{L}}} \\ \bar{\mathbf{L}} & = & \mathbf{k}_b\, L \end{array}$$

and

$$\mathbf{k_b}(\omega) = \sqrt{\omega}\left(\frac{\rho\, A}{E\, I}\right)^{\frac{1}{4}}. \tag{5}$$

The dynamic stiffness matrix of the structure members ROC for the axial–bending beam model can be obtained by combining the rod and beam spectral element given by Eq. (1), where

$$\mathbf{u} = \begin{bmatrix} u_1 & w_1 & \phi_1 & u_2 & w_2 & \phi_2 \end{bmatrix}^T, \tag{6}$$

$$\mathbf{F} = \begin{bmatrix} N_1 & V_1 & M_1 & N_2 & V_2 & M_2 \end{bmatrix}^T \tag{7}$$

and

$$\mathbf{S_f} = \begin{bmatrix} S_{r11} & 0 & 0 & S_{r12} & 0 & 0 \\ 0 & S_{b11} & S_{b12} & 0 & S_{b13} & S_{b14} \\ 0 & S_{b21} & S_{b22} & 0 & S_{b23} & S_{b24} \\ S_{r21} & 0 & 0 & S_{r22} & 0 & 0 \\ 0 & S_{b31} & S_{b32} & 0 & S_{b33} & S_{b34} \\ 0 & S_{b41} & S_{b32} & 0 & S_{b43} & S_{b44} \end{bmatrix}, \tag{8}$$

where the subscripts r and b denote the components of the spectral element matrices for the rod element and Bernoulli–Euler beam element, $\mathbf{u}$ is the spectral nodal degrees-of-freedom vector, and $\mathbf{F}$ is the spectral nodal generalized forces vector. The u_i, w_i and ϕ_i $(i = 1, 2)$ are the spectral components of the nodal axial and transverse displacements, and rotations. The N_i, V_i and M_i $(i = 1, 2)$ are the spectral components of the nodal internal axial, transverse shear forces, and bending moments, respectively. The spectral nodal degrees-of-freedom $\mathbf{u}$ in the local coordinates can be related to the spectral nodal degrees-of-freedom $\mathbf{u_g}$ in the global coordinates through,

$$\mathbf{\Psi} = \begin{bmatrix} \cos(\theta) & -\sin(\theta) & 0 & 0 & 0 & 0 \\ \sin(\theta) & \cos(\theta) & 0 & 0 & 0 & 0 \\ 0 & 0 & 1 & 0 & 0 & 0 \\ 0 & 0 & 0 & \cos(\theta) & -\sin(\theta) & 0 \\ 0 & 0 & 0 & \sin(\theta) & \cos(\theta) & 0 \\ 0 & 0 & 0 & 0 & 0 & 1 \end{bmatrix}, \tag{9}$$

where $\mathbf{\Psi}$ is the local-to-global coordinate transformation matrix and θ is the rotation angle of the local coordinates measured counterclockwise. The dynamic stiffness matrix of the structure members ROC ($\mathbf{S}$), can be obtained in global coordinates as follows:

$$\mathbf{S} = \mathbf{\Psi^T}\, \mathbf{S_f}\, \mathbf{\Psi}. \tag{10}$$

Spectral element using transfer method

WSE method uses the concept of transfer matrix methods to compute the wave modes along periodic structures. The PC structure are assumed to be 1D periodic coupling waveguides (beams) in the sense that they are composed of identical

substructures - which are made with two alternate directions. By considering the wave modes, the frequency forced response of periodic structures can be computed in an efficient way.

Equation (1) can be partitioned in terms of left (L) and right (R) boundaries to obtain the WSE transfer matrix formulation as:

$$\underbrace{\begin{Bmatrix} \mathbf{u}_{\mathtt{R}} \\ -\mathbf{F}_{\mathtt{R}} \end{Bmatrix}}_{\mathbf{q}_R} = \underbrace{\begin{bmatrix} -\mathbf{S}_{\mathtt{LR}}^{-1}\mathbf{S}_{\mathtt{LL}} & -\mathbf{S}_{\mathtt{LR}}^{-1} \\ \mathbf{S}_{\mathtt{RL}} - \mathbf{S}_{\mathtt{RR}}\mathbf{S}_{\mathtt{LR}}^{-1}\mathbf{S}_{\mathtt{LL}} & -\mathbf{S}_{\mathtt{RR}}\mathbf{S}_{\mathtt{LR}}^{-1} \end{bmatrix}}_{\mathbf{T}} \underbrace{\begin{Bmatrix} \mathbf{u}_{\mathtt{L}} \\ \mathbf{F}_{\mathtt{L}} \end{Bmatrix}}_{\mathbf{q}_L}, \tag{11}$$

where $\mathbf{q}_i = \{\mathbf{u}_i \quad \mathbf{F}_i\}^T$ with $i = \mathtt{L}, \mathtt{R}$ are the state-space vectors, $\mathbf{T}$ is the WSE transfer matrix of a cell (Figure 2).

Wave spectral element method

Consider a one-dimensional periodic homogeneous structure or a phononic crystal (Figure 2), where each periodic substructure or unit-cell is coupled to its neighbors on each boundary by a displacement vector $\mathbf{u}$, and a force vector $\mathbf{F}$. The transfer matrix solution can be formulated in terms of left-hand (L) and right-hand boundary (R) of a cell by:

$$\mathbf{q}_{\mathtt{R}} = \mathbf{T}\mathbf{q}_{\mathtt{L}} \tag{12}$$

where $\mathbf{q}_{\mathtt{B}} = \{\mathbf{u}_{\mathtt{B}} \quad \mathbf{F}_{\mathtt{B}}\}^T$ is the state-space vectors at the boundary $\mathtt{B} = \mathtt{L}, \mathtt{R}$, and $\mathbf{T}$ is the $[2n \times 2n]$ transfer matrix with n as the number of degrees of freedom (DOFs) in the left or right boundary of the considered unit-cell.

By applying displacement condition and force balance for consecutive cells $m-1$ and m it has,

$$\begin{cases} \mathbf{u}_{\mathtt{L}}{}^{(m)} = \mathbf{u}_{\mathtt{R}}{}^{(m-1)} \\ \mathbf{F}_{\mathtt{L}}{}^{(m)} = -\mathbf{F}_{\mathtt{R}}{}^{(m-1)} \end{cases} \quad \text{or} \qquad \mathbf{q}_{\mathtt{L}}{}^{(m)} = \mathbf{q}_{\mathtt{R}}{}^{(m-1)}. \tag{13}$$

Substituting Eq.(13) in the Eq.(12) produces,

$$\mathbf{q}_{\mathtt{L}}^{(m)} = \mathbf{T}\mathbf{q}_{\mathtt{L}}^{(m-1)}. \tag{14}$$

For a infinite number of unit-cells the Bloch-Floquet's theorem (Mead, 1970) can be applied to obtain,

$$q_L^{(m)} = e^{\mu} q_L^{(m-1)} \tag{15}$$

where $\mu = -\mathtt{i}k_B L_c$ is the attenuation constant, k_B is the Bloch wavenumber, L_c is the unit-cell length and $\mathtt{i}$ is the imaginary number. Substituting Eq.(15) in the Eq.(14) and disregarding the unit-cell index (m), it has,

$$\mathbf{T}\mathbf{q} = e^{\mu}\mathbf{q} \tag{16}$$

which is the Bloch wave eigenproblem, that can be rewritten as:

$$\mathbf{T}\phi_j = \beta_j \phi_j, \tag{17}$$

where $\beta_j = e^{\mu_j}$ is the $j-th$ eigenvalue that produces the Bloch wavenumber k_j, and ϕ_j is the corresponding eigenvector that represents the Bloch wave mode shape. These solutions can be refereed as β_j, ϕ_j and it means that Bloch wave modes propagates along the whole structure. Since structural systems produce symplectic transfer matrices there are n right-propagating (incident) wave modes (β_j, ϕ_j) where $|\beta_j| < 1$ and n left-propagating (reflected) wave modes (β_j^*, ϕ_j^*) where $\beta_j^* = 1/\beta_j$. It must also be noted that each eigenvector ϕ_j can be written as a function of the wave displacement and wave force components as $\phi_j = \{\phi_{u_j} \; \phi_{F_j}\}^T$. Then, the wave basis can be expressed in matrix form as:

$$\mathbf{\Phi} = \begin{bmatrix} \mathbf{\Phi}_u & \mathbf{\Phi}_u^* \\ \mathbf{\Phi}_F & \mathbf{\Phi}_F^* \end{bmatrix}, \tag{18}$$

where $\mathbf{\Phi}_u$, $\mathbf{\Phi}_F$, $\mathbf{\Phi}_u^*$, and $\mathbf{\Phi}_F^*$, are $[n \times n]$ wave modes matrices where superscripts without and with asterisk $(*)$ refer to as positive and negative wave-going, respectively. While the subscripts u and F refer to as displacement and force components, respectively. The $\boldsymbol{\beta} = diag(\beta_j)$ and $\boldsymbol{\beta^*} = \boldsymbol{\beta}^{-1}$ are the eigenvalue matrices of incident and reflected modes, respectively.

However, the WSE transfer matrix $\mathbf{T}$ for large structures can produce an eigenproblem with numerical difficulties Waki *et al.* (2009), which needs to be recast into one better-conditioned. For this case, the space-state vector in the Eq. (11) can be rewritten as a displacement vector alone by (Zhong and Williams, 1995) and the transfer matrix conditioning can be improved as:

$$\beta_j \underbrace{\begin{bmatrix} \mathbf{I}_n & \mathbf{0} \\ -\mathbf{S}_{\mathtt{LL}} & -\mathbf{S}_{\mathtt{LR}} \end{bmatrix}}_{\mathbf{L}} \underbrace{\begin{Bmatrix} \mathbf{u}_{\mathtt{L}} \\ \mathbf{u}_{\mathtt{R}} \end{Bmatrix}}_{\mathbf{w}_j} = \underbrace{\begin{bmatrix} \mathbf{0} & \mathbf{I}_n \\ \mathbf{S}_{\mathtt{RL}} & \mathbf{S}_{\mathtt{RR}} \end{bmatrix}}_{\mathbf{N}} \underbrace{\begin{Bmatrix} \mathbf{u}_{\mathtt{L}} \\ \mathbf{u}_{\mathtt{R}} \end{Bmatrix}}_{\mathbf{w}_j} \tag{19}$$

where $\mathbf{w}_j$ are the eigenvectors associated to the cell. It can also be shown that the eigenvectors of Eq. (17) are $\phi_j = \mathbf{L}\mathbf{w}_j$.

2.1.1 Wave mode expansion

Consider a periodic structure or a phononic crystal composed by N unit-cells, then the number of interfaces are $N+1$. The displacement and forces of a unit-cell m are expanded in a wave basis that results in:

$$\begin{aligned} \mathbf{u}^{(m)} &= \mathbf{\Phi}_u \mathbf{Q}^{(m)} + \mathbf{\Phi}_u^* \mathbf{Q}^{*(m)}, \\ \pm\mathbf{F}^{(m)} &= \mathbf{\Phi}_F \mathbf{Q}^{(m)} + \mathbf{\Phi}_F^* \mathbf{Q}^{*(m)}, \end{aligned} \tag{20}$$

where $\mathbf{Q}^{(m)}$ and $\mathbf{Q}^{*(m)}$ are the wave amplitude at the $m-th$ cell interface and $\pm F$ indicates the force orientation.

It can be shown that the spatial distribution of the wave amplitude is given by Mencik (2010):

$$\begin{aligned} \mathbf{Q}^{(m)} &= \boldsymbol{\beta}^{(m-1)} \mathbf{Q}^{(1)}, \\ \mathbf{Q}^{*(m)} &= \boldsymbol{\beta}^{*(m-1-N)} \mathbf{Q}^{*(1)}, \end{aligned} \tag{21}$$

with $m = 1, \ldots, N+1$. Replacing the Equation (21) into Equation (20) and considering that $\boldsymbol{\beta}^* = 1/\boldsymbol{\beta}$, it has:

$$\begin{aligned} \mathbf{u}^{(m)} &= \mathbf{\Phi}_u \boldsymbol{\beta}^{(m-1)} \mathbf{Q} + \mathbf{\Phi}_u^* \boldsymbol{\beta}^{(N+1-m)} \mathbf{Q}^*, \\ \pm\mathbf{F}^{(m)} &= \mathbf{\Phi}_F \boldsymbol{\beta}^{(m-1)} \mathbf{Q} + \mathbf{\Phi}_F^* \boldsymbol{\beta}^{(N+1-m)} \mathbf{Q}^*. \end{aligned} \tag{22}$$

The wave amplitude $\mathbf{Q}$ and $\mathbf{Q}^*$ can be determined considering the boundary condition. Considering N cells and applying Neumann and Dirichlet boundary conditions, left ($m = 1$) and right ($m = N+1$) ends are respectively submitted to forces and displacements in the Eq. (22) to obtain:

$$\begin{aligned} \mathbf{\Phi}_F \mathbf{Q} + \mathbf{\Phi}_F^* \boldsymbol{\beta}^N \mathbf{Q}^* &= -\mathbf{F}^{(1)} = -\mathbf{F}_0 \\ \mathbf{\Phi}_u \boldsymbol{\beta}^N \mathbf{Q} + \mathbf{\Phi}_u^* \mathbf{Q}^* &= \mathbf{u}^{(N+1)} = \mathbf{u}_0. \end{aligned} \tag{23}$$

which can be written in matrix form and rearranged to obtain the wave amplitudes as:

$$\begin{Bmatrix} \mathbf{Q} \\ \mathbf{Q}^* \end{Bmatrix} = \begin{bmatrix} \mathbf{\Phi}_F & \mathbf{\Phi}_F^* \boldsymbol{\beta}^N \\ \mathbf{\Phi}_u \boldsymbol{\beta}^N & \mathbf{\Phi}_u^* \end{bmatrix}^{-1} \begin{Bmatrix} -\mathbf{F}_0 \\ \mathbf{u}_0 \end{Bmatrix} \tag{24}$$

Ill-conditioning of the matrix to be inverted in Eq. (24) is likely to occur. An alternative solution is multiplying Eq.(24) by the vector $[\mathbf{\Phi}_F^{-1} \ \mathbf{\Phi}_u^{*-1}]^T$ to obtain:

$$\begin{Bmatrix} \mathbf{Q} \\ \mathbf{Q}^* \end{Bmatrix} = \begin{bmatrix} \mathbf{I} & \mathbf{\Phi}_F^{-1} \mathbf{\Phi}_F^* \boldsymbol{\beta}^N \\ \mathbf{\Phi}_u^{*-1} \mathbf{\Phi}_u \boldsymbol{\beta}^N & \mathbf{I} \end{bmatrix}^{-1} \begin{Bmatrix} -\mathbf{\Phi}_F^{-1} \mathbf{F}_0 \\ \mathbf{\Phi}_u^{*-1} \mathbf{u}_0 \end{Bmatrix} \tag{25}$$

By knowing the wave amplitudes the forced response of a structure composed of N identical unit-cells can be obtained.

3. NUMERICAL RESULTS

In this section, the waveguides frame are coupled in triangular form with $\theta = 0$, $\pi/12$ and $\pi/4$. The forced response is calculated using SEM, SEM with TM and WSEM. Material properties used for this simulation are: $E_{\text{steel}} = 210\,\text{GPa}$, $\rho_{\text{steel}} = 7800\,\text{kg/m}^3$, $\nu = 0.3$, $\eta = 0.01$. Member dimensions are: length ($L = 0.05$ m), height ($h = 0.01$ m), and width ($b = 0.005$ m). The results are computed for a structure formed by six cells with free-free boundary conditions. It was excited at the free end with a unitary force in "y" direction.

In the first result it was obtained the dispersion diagram of a cell (Fig. 2) as can be seen in the Fig. 3 from of WSEM. Curves are the real (blue) and imaginary (red) parts of the wavenumber. In this figure is shown the results for three configurations of this cell, where the difference between them is the coupling angle θ. Plot in Fig. 3.(a) shows results for a cell with $\theta = 0$, whereas for the Fig. 3.(b) the cell has $\theta = \pi/12$, and in Fig. 3.(c), cell has $\theta = \pi/4$. It is possible to observe something like a band gap at frequencies around 1 kHz for $\theta = \pi/12$ and $\pi/4$ in highlight area in the Fig. 3. Furthermore, this likely attenuation effect increases as the angle θ approaches $\pi/2$. However, the behavior is slightly different from what normally occurs in Bragg scatterings known until then. In this case, the attenuation did not occur at Bragg limits. It seems that the modes have not stopped propagating, however, part of these two modes (longitudinal and flexural) became evanescent.

In Fig. 4 is shown two attenuation curves (Xiao *et al.* (2012); Nobrega *et al.* (2016)) for which the band frequencies coincide with the evancescents waves presented in the highlighted area in Fig. 3. It is possible see that the attenuation increase as θ rise (Fig.3(a) and 3(b)). Even more, another gap started to open close to 3 kHz as expected in a typical Bragg scattering.

To confirm the existence of this band gap due to the Bragg scattering, the forced responses of the structure for the three cases ($\theta = 0$, $\theta = \pi/12$ and $\theta = \pi/4$) were calculated, as can be seen in Fig. 5. The curves shown in the figure follow

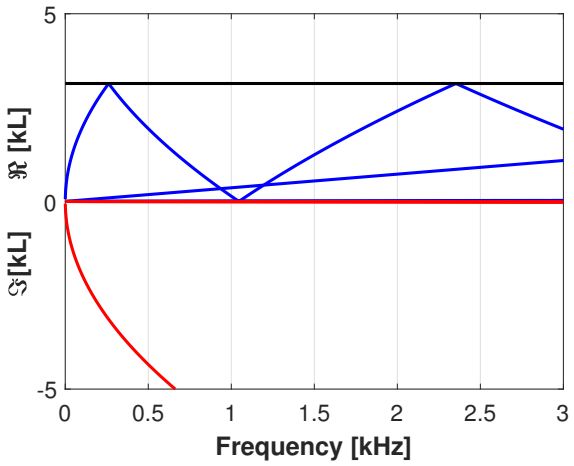

(a) $\theta = 0$

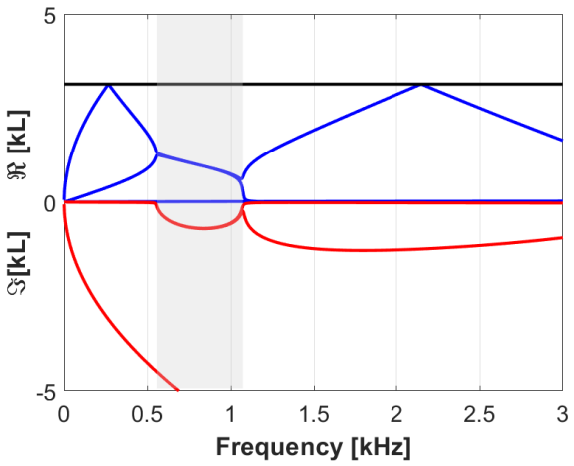

(b) $\theta = \pi/12$

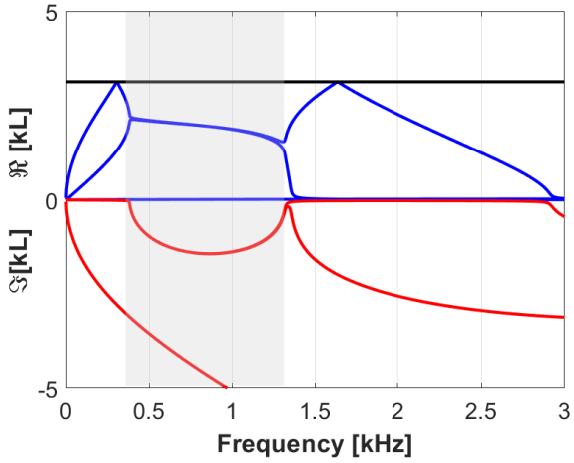

(c) $\theta = \pi/4$

Figure 3. The real (blue) and and imaginary (red) parts of the dispersion diagram of the cell frame with $\theta = 0,\ \pi/12$ and $\pi/4$. The black straight-line is the Bragg limit. The highlight area represent the band gap width and position.

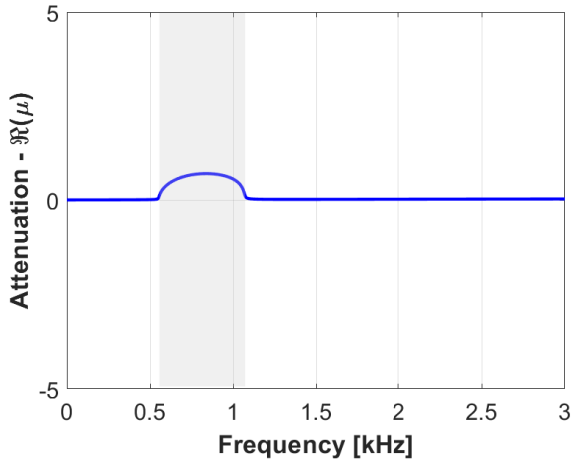

(a) $\theta = \pi/12$

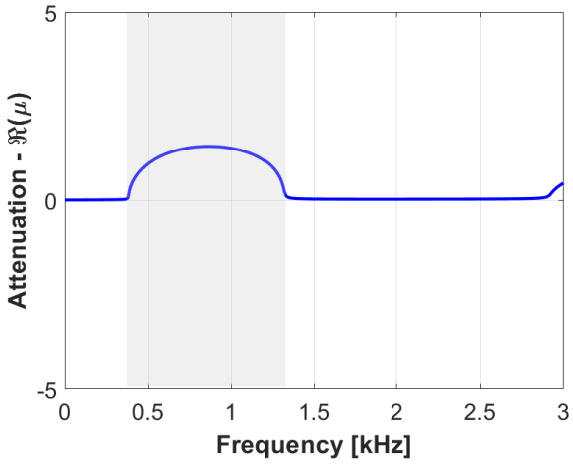

(b) $\theta = \pi/4$

Figure 4. Attenuation of the cell with $\theta = \pi/12$ and $\pi/4$. The highlight area represent the band gap width and position.

the same pattern as the previous ones (Fig. 3). Another observation that can be made is about the band gap shape in Fig.

5. Normally, they have the same format of the evanescent wave (like a semi-elliptical curve) for PC structures. However, in this case, they appear with some anti-resonances that only occur when there are propagating and evanescent waves in the same band frequency of the band gaps.

Finally, SEM, SEM TM and WSEM were used to validate the results. As can be seen, they agree well in all band frequencies, except for the SEM TM where the results start to approach the singularity and the curve starts to present inconsistent results.

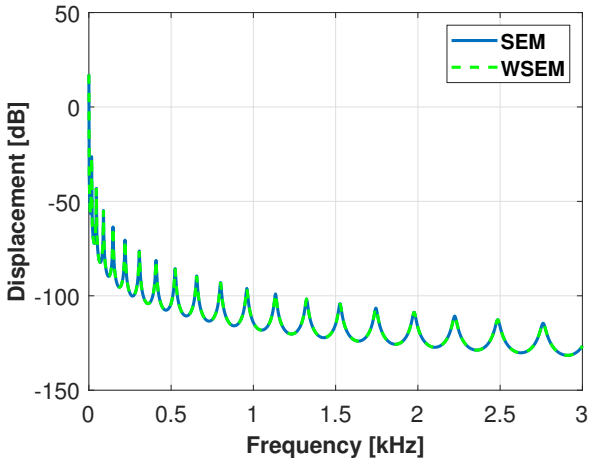

(a) $\theta = 0$

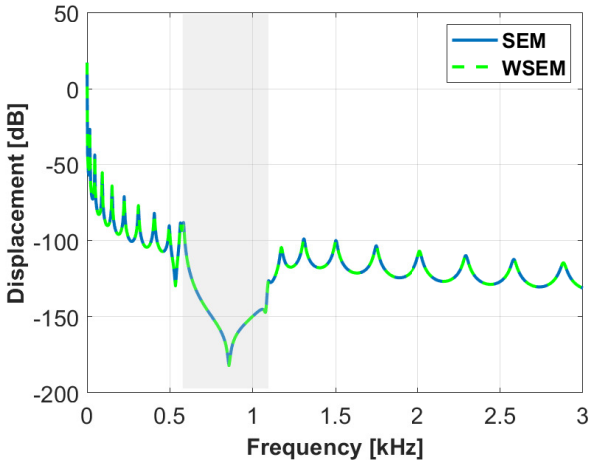

(b) $\theta = \pi/12$

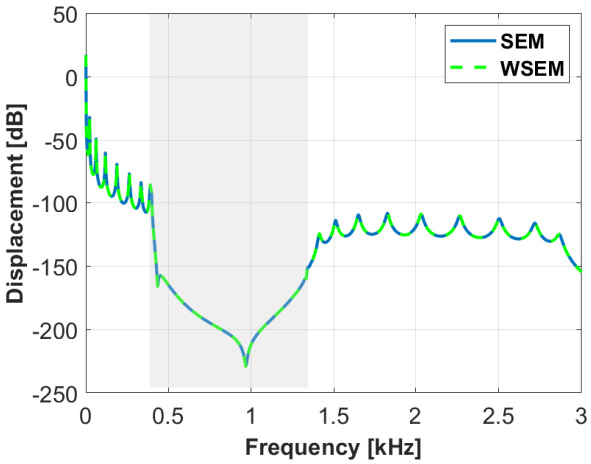

(c) $\theta = \pi/4$

Figure 5. Displacement in the opposite edge of the excitation. This frame have the same material and $\theta = 0,\ \pi/12$ and $\pi/4$. The highlight area represent the band gap width and position.

4. CONCLUSION

This work presented an analysis of a origami-like structure that was formed of repeating triangular cells. Results obtained for three different angles of members coupling using SEM, and WSEM, successfully identified band gaps frequencies, which ranges increased for bigger coupling angles. Also, dispersion diagrams and attenuation results shown agreement for the identification of band gaps frequency ranges.

5. ACKNOWLEDGEMENTS

The authors are grateful to the Brazilian research funding agencies FAPEMA, FAPESP (Grant no. 2018/15894-0) , FAPEMIG, CNPq (Grant no. 313620/2018), and CAPES for their financial support.

6. REFERENCES

Chen, P., Wang, Y.Z. and Wang, Y.S., 2020. "Active control of flexural waves in a phononic crystal beam with staggered periodic properties". *Wave Motion*, Vol. 93, p. 102481. doi:10.1016/j.wavemoti.2019.102481.

Goto, A.M., Nóbrega, E.D., Pereira, F.N. and Santos, J.M.C.D., 2020. "Numerical and experimental investigation of phononic crystals via wave-based higher-order rod models". *International Journal of Mechanical Sciences*, Vol. 181, p. 105776. doi:10.1016/j.ijmecsci.2020.105776.

Hussein, M.I., Leamy, N.J. and Ruzzene, M., 2014. "Dynamics of phononic materials and structures: Historical origins, recent progress, and future outlook". *Applied Mechanics Reviews (Trans. ASME)*, Vol. 66, p. 38pp.

Lee, U., 2009. *Spectral element method in structural dynamics*. John Wiley and Sons (Asia).

Lv, C., Krishnaraju, D., Konjevod, G., Yu, H. and Jiang, H., 2014. "Origami based mechanical metamaterials". *Scientific Reports*, Vol. 4, No. 1. doi:https://doi.org/10.1038/srep05979.

Mead, D.J., 1970. "Free wave propagation in periodically supported, infinte beams". *Journal of Sound and Vibration*, Vol. 11(2), pp. 181–197.

Mead, D.J., 1973. "A general theory of harmonic wave propagation in linear periodic systems with multiple coupling". *Journal of Sound and Vibration*, Vol. 27(2), pp. 235–260.

Mencik, J.M., 2010. "On the low- and mid-frequency forced response of elastic structures using wave finite elements with one-dimensional propagation". *Computers and Structures*, Vol. 88, pp. 674–689.

Miranda, E.J.P., Nobrega, E.D., Ferreira, A.H.R. and Santos, J.M.C.D., 2019. "Flexural wave band gaps in a multi-resonator elastic metamaterial plate using kirchhoff-love theory". *Mechanical Systems and Signal Processing*, Vol. 116, pp. 480–504. doi:10.1016/j.ymssp.2018.06.059.

Miranda, E.J.P., Nobrega, E.D., Rodrigues, S.F., Aranas, C. and Santos, J.M.C.D., 2020. "Wave attenuation in elastic metamaterial thick plates: Analytical, numerical and experimental investigations". *International Journal of Solids and Structures*, Vol. 204-205, pp. 138–152. doi:10.1016/j.ijsolstr.2020.08.002.

Nanda, A. and Karami, M., 2018. "Tunable bandgaps in a deployable metamaterial". *Journal of Sound and Vibration*, Vol. 424, pp. 120–136. doi:10.1016/j.jsv.2018.03.015.

Nobrega, E., Gautier, F., Pelat, A. and Santos, J.D., 2016. "Vibration band gaps for elastic metamaterial rods using wave finite element method". *Mechanical Systems and Signal Processing*, Vol. 79, pp. 192–202. doi:10.1016/j.ymssp.2016.02.059.

P B Silva, J R F Arruda and A L Goldstein, 2011. "Study of elastic band-gaps in finite periodic structure using finite element models". doi:10.13140/2.1.1793.6641.

Pereira, F.N. and Santos, J.M.C.D., 2021. "Phononic crystal investigation using a fluid-structure circular cylindrical shell spectral element". *Mechanical Systems and Signal Processing*, Vol. 148, p. 107100. doi:10.1016/j.ymssp.2020.107100.

Silva, P.B., Goldstein, A.L. and Arruda, J.R.F., 2013. "Building spectral element dynamic matrices using finite element models of waveguide slices and elastodynamic equations". *Shock and Vibration*, Vol. 20, p. 439–458.

Waki, Y., Mace, B. and Brennan, M.J., 2009. "Numerical issues concerning the wave and finite element method for free and forced vibrations of waveguides". *Journal of Sound and Vibration*, Vol. 327, pp. 92–108.

Xiao, Y., Wen, J. and Wen, X., 2012. "Longitudinal wave band gaps in metamaterial-based elastic rods containing multi-degree-of-freedom resonators". *New Journal of Physics*, Vol. 14, p. 20.

Xiao, Y., Wen, J. and Wen, X., 2013. "Flexural vibration band gaps characteristics in phononic crystal euler beams on two-parameter foundation". *Advances in Mechanical Engineering*, Vol. 2013, p. 7.

Zhong, W.X. and Williams, F.W., 1995. "On the direct solution of wave propagation for repetitive structures". *Journal of Sound and Vibration*, Vol. 182(3), pp. 485–501.

7. RESPONSIBILITY NOTICE

Author are solely responsible for the printed material included in this paper.